Journal of Molecular Liquids 400 (2024) 124496

Contents lists available at ScienceDirect

Journal of Molecular Liquids

journal homepage: www.elsevier.com/locate/molliq

Tuning the bulk behavior and 2D interfacial self-assembly of microgels by keggin-type polyoxometalate ionic specificity

Antonio Rubio-Andrés, Delfi Bastos-González, Miguel Angel Fernandez-Rodriguez *

Laboratory of Surface and Interface Physics, Biocolloid and Fluid Physics Group, Department of Applied Physics, Faculty of Sciences, University of Granada, Granada, 18071, Spain

ARTICLE INFO

Keywords:
Microgels
Keggin-type polyoxometalates
Interface
Ion specificity
Self-assembly
Soft colloidal lithography

ABSTRACT

Finding new ways to tune the behavior of thermoresponsive microgels in bulk and confined at 2D liquid interfaces is key to achieve a deeper understanding and control of these smart materials. We studied the interaction of positively and negatively charged pNIPAM microgels with the Keggin-type polyoxometalates $Na_3PW_{12}O_{40}$ (POM^{3-}) and $H_4SiW_{12}O_{40}$ (POM^{4-}). In bulk, we observed charge inversions of the positively charged microgels below and above the volume phase transition temperature (VPTT) at significantly low POM concentrations as $5 \cdot 10^{-5}$ M. In the presence of POM, both microgels exhibited a deswelling-swelling-deswelling behavior below the VPTT, and a two-step further deswelling above the VPTT for the positively charged microgels. When the later were confined at 2D water/air interfaces, adding 10^{-5} M of POM^{3-} below the VPTT was equivalent to heating above the VPTT and compressing the monolayer from 5 to 20 mN m^{-1}. Above the VPTT, the diameter at the interface did not change while the portion immersed in the subphase further deswelled, in agreement with the behavior in bulk. Adding more POM^{3-} did not change the diameter at the interface nor the height of the microgels, showing a saturation effect in 2D. The restructuring of the pNIPAM polymeric network by the POM^{3-} was characterized by EDS mapping and XPS. The microgel monolayers with POM^{3-} improved their resistance to plasma etching, which could be useful for soft colloidal lithography.

1. Introduction

Microgels are soft colloidal micro- and nanoparticles composed of cross-linked polymers that are swollen in a good solvent. Poly-(N-isopropylacrylamide) (pNIPAM) microgels dispersed in water are widely used thanks to their thermoresponsiveness, exhibiting a Volume Phase Transition Temperature (VPTT). The microgel swells below the VPTT and deswells above it, expelling water and stiffening in the process. [1]. It is possible to tune their response to other external stimuli during the synthesis, e.g. they can become pH-responsive by adding amphoteric co-monomers [2,3].

One of the usual synthesis routes to obtain pNIPAM microgels is the precipitation polymerization, where they develop a Gaussian profile on the cross-linking density, with a highly cross-linked core and a less cross-linked corona [4–6]. When a microgel adsorbs at a liquid interface, the portion in contact with the interface stretches due to the surface tension, only counterbalanced by the internal elasticity of the polymeric network, which it is proportional to the cross-linking density. As a result, the microgel exhibits a *fried-egg* shape when it is seen from above the interface, with the portion below the subphase still well solvated [7,8].

When confined at interfaces, microgels can be used as Pickering emulsion stabilizers, where their responsiveness allows to destabilize the emulsions by the influence of an external stimulus [9,10]. Moreover, when transferred to a silicon substrate, the deposited microgels can perform as lithography masks for soft colloidal lithography, to fabricate arrays of vertically aligned silicon nanowires [11]. In this process, the silicon is etched by Deep Reactive Ion Etching (Deep-RIE). During this process, it is the complete etching of the microgels acting as lithography masks what determines the upper boundary for the height of the vertically aligned nanowires.

In order to improve their performance in these or any other applications, we need to gain a deeper understanding of the behavior of microgels confined at fluid interfaces. Indeed, the portion of the microgel still immersed in the water subphase will keep its responsiveness to external stimuli, while the portion stretched at the interface will be mainly dominated by the surface tension [3,12,13]. Concerning the thermoresponsiveness, the diameter of the microgel at the inter-

* Corresponding author.
E-mail address: mafernandez@ugr.es (M.A. Fernandez-Rodriguez).

https://doi.org/10.1016/j.molliq.2024.124496
Received 25 August 2023; Received in revised form 12 March 2024; Accepted 14 March 2024
Available online 24 March 2024

face remains the same regardless of the temperature. Nevertheless, as it occurs for microgels in bulk, the portion immersed in the water subphase deswells above the VPTT, decreasing the diameter of that portion [12–15]. Upon deposition on a substrate, this deswelling results in an increase of the microgel height [12].

Recently, Schmidt et al. showed that for pH-responsive microgels confined at fluid interfaces the behavior is different upon pH-swelling/deswelling depending on the size of the microgel [3]. For big microgels (e.g. 800 nm) they found a similar behavior compared to that found for the thermoresponsiveness, with invariable diameter at the interface while the portion immersed in the water subphase was still pH-responsive. Interestingly, for small microgels (e.g. 250 nm) the diameter at the interface decreased upon pH-swelling of the microgels.

Another tool that can be used to tune the properties of microgels in dispersion, e.g. their charge and size, is the addition of salt. While this provides electrostatic screening of charges, we will particularize here to ionic specific interactions. The influence of the ionic specificity on pNIPAM has been widely analyzed in bulk for both free chains and microgels [16–18]. In both cases, the properties of pNIPAM are deeply affected by salts belonging to the Hofmeister series, specially when anions act as counter-ions [19,20]. However, there is a lack of experimental works studying how salts influence the interfacial properties of pNIPAM, probably due to the difficulty in obtaining reliable and accurate data in 2D systems.

There are many interesting ions candidates with complex behaviors, such as cobaltabisdicarbollide anions, but these exhibit interfacial activity [21], and therefore they would compete with the adsorption of microgels at interfaces. An interesting kind of anions are the Keggin-type polyoxometalates (POMs), nanosized metal-oxide clusters with high valences and well defined structures [22]. They do not exhibit interfacial activity by themselves, but they can adsorb at the interface in the presence of interfacially active molecules [23,24]. Moreover, they can induce the self-assembly of free pNIPAM chains in bulk into sheets and globules [22,25], but a comprehensive study on how this effect translates to microgels, both in bulk and at interfaces, is only recently starting to be studied [26].

This strong interaction of POMs with pNIPAM has been observed also with proteins and seems difficult to be modeled by classical models. Recently, it has been proposed a quantum description of the interaction [27]. The parallelism with proteins comes from the amide groups of pNIPAM that resemble the aminoacid structure. Furthermore, POMs have been gaining attention due to their interesting and versatile applications, from their use in catalytic reactions [28], anticancer drugs [29], hybrid antimicrobial materials [30], or pollution removal [31] to cite some applications.

In this work, we explore the role of the ionic specificity of the Keggin-type polyoxometalates $Na_3PW_{12}O_{40}$ (POM^{3-}), $H_4SiW_{12}O_{40}$ (POM^{4-}) ions, and pNIPAM microgels, both in bulk and at the water/air interface. In bulk, by means of laser Doppler microelectrophoresis and Dynamic Light Scattering (DLS) size measurements, and at the water/air interface, from monolayer deposition and AFM, TEM, STEM-HAADF, EDS and XPS characterizations. Finally, we briefly explore a potential application in Soft Colloidal Lithography of the pNIPAM microgel monolayers deposited in the presence of the POM^{3-} by testing their resistance to plasma etching.

2. Materials and methods

2.1. Materials

The pNIPAM microgels were synthesized as reported in a previous work by precipitation polymerization [19]. Further details are provided in the Supporting Materials. We used Milli-Q water in all our experiments. N-Isopropylacrylamide (NIPAM), aminoethyl methacrylate hydrochloride (AEMH), N-methylenebisacrylamide (BIS) and 2,2'-azobis (2-amidinopropane) dihydrochloride (V50) were obtained from Acros in analytical grade and used as received. The POM^{3-} $Na_3PW_{12}O_{40}$ (Sigma Aldrich, 99.9%), $H_4SiW_{12}O_{40}$ (POM^{4-}, Sigma Aldrich, anhydrous base), NaOH (Acros Organics, for analysis), HCl (Sigma Aldrich, ACS reagent 37%), and NaCl (Sigma Aldrich, 99%) were used as received. Isopropyl alcohol (Sigma Aldrich, 99.8%) was used as extension agent for the experiments at the water/air interfaces. Silicon substrates of 2 x 1 cm^2 with ⟨100⟩ orientation (p-type, Boron doped, 1-10 Ω cm from University Wafer Inc., USA) were cut by laser (Laser E-20 SHG II, Rofin, USA) and used for the deposition of microgel monolayers without further modification.

2.2. Sample preparation and physicochemical characterization in bulk

The pH 3 Milli-Q water used in all experiments was prepared by adjusting the pH of Milli-Q water with HCl. It was found that the pH-probe was a source of contamination for the interfacial experiments. To avoid cross-contamination from the pH-probe, few drops of HCl were added to the Milli-Q water. Then, a fraction was extracted and the pH was measured. This process was repeated until pH 3 was reached. Then, a $20 \cdot 10^{-3}$ M stock POM^{3-} and POM^{4-} solution was prepared by diluting the POM on freshly prepared pH 3 Milli-Q water. After the addition of POM, the pH could differ from pH 3. Therefore, either NaOH or HCl was added dropwise to adjust it to pH 3. To prepare the POMs solutions, the POMs stock solutions was diluted on the pH 3 Milli-Q water to the desired POMs concentration. Although at this pH the POM^{3-} is not completely stable [32,33], and lacunary species such as $PW_{11}O_{39}^{7-}$ might be present, pH 3 was chosen to increase the range of applicability of our system, since the POM^{3-} was weakly affected by working at this pH.

The hydrodynamic diameter (D_h) and the electrophoretic mobility (μ_e) were measured via a ZetaSizer NanoZ (Malvern Instruments, UK). All the measurements were performed at temperatures between 25 °C and 50 °C to investigate the swollen and deswollen states of the microgels, respectively. The results were obtained by the average of three measurements and their corresponding standard deviations. For each characterization, a microgel solution of 0.1 wt% was prepared 15 minutes prior to the measurement. When the desired temperature was achieved, the sample was stabilized during 3 minutes before starting the experiments. The VPTT was obtained from a sigmoidal fit of the evolution of the D_h as a function of the temperature in the absence of salt, as detailed in the Supplementary Materials (see Fig. S1 and S2).

2.3. Langmuir trough depositions

Details on silicon substrate sample preparation, cleaning protocols, Langmuir trough (KSV NIMA, Biolin Scientific, Sweden) barrier compression and dipping speeds are detailed in the Supplementary Materials. It is known that the deposition method can affect the microgel shape and conformation on the solid substrate [34]. In order to offer meaningful comparisons, we restricted to a widely used and standardized deposition method which provides reproducible results [12,11]. First, a silicon substrate was attached to the dipper arm of the Langmuir trough and lowered below the interface position at an angle of 60°. The clean Langmuir trough was then filled with the desired ionic solution at pH 3, and heated above the VPTT when needed thanks to a thermal bath heating the trough from outside. When the interface was considered clean enough (see Supplementary Materials), the microgel suspension was deposited at the interface thanks to a 100 μL glass microsyringe, up to a surface pressure of $\Pi \simeq 1$ mN m^{-1}, allowing it to equilibrate for 10 minutes. Next, we performed two types of experiments. The first type was intended to characterize the compression curve of the microgel. In this case the monolayer was compressed while simultaneously lifting the substrate across the interface. Just before the substrate completely crossed the interface, the barriers were fully opened to create a sudden change in Π which we used as a reference point to match each position on the substrate with its corresponding surface pressure via AFM

[12]. In this way, it is possible to reconstruct the compression curve by representing Π as a function of the area occupied by each microgel. The other type of experiment was intended to investigate the effect of the POM^{3-} concentration on the self-assembly of the microgel monolayer. First, the monolayer was compressed up to $\Pi = 5\,mN\,m^{-1}$ and deposited on half of the substrate. Next, the monolayer was compressed up to $\Pi = 20\,mN\,m^{-1}$ and deposited on the rest of the substrate. In this way, there were two different areas over the substrate corresponding to the two values of Π. After each deposition experiment, the Langmuir trough was cleaned as detailed in Supplementary Materials.

2.4. AFM and image analysis

The deposited monolayers were characterized by means of Atomic Force Microscopy (AFM, motorized Dimension 3000) in tapping mode (Tap300Al-G cantilevers, 300 kHz, 40 N/m, BudgetSensors, Bulgaria). We acquired 512 x 512 $pixels^2$ images of 40 x 40 μm^2 and 10 x 10 μm^2 over the microgel monolayers deposited on the silicon substrates. For the compression curve, we acquired images every 500 μm over the substrate from the reference point thanks to a customized motorization of the AFM [35]. For the substrates with two regions at 5 and 20 $mN\,m^{-1}$, we acquired images of each region. The images were post-processed with the software Gwyddion to level them and increase contrast. Next, the images were converted to 8-bits grey-scale images and analyzed using a customized particle tracking software based on the Python version of the publicly available particle tracking code by Crocker and Grier TrackPy [36]. Thus, we localized the center of each particle excluding the microgels placed in the edges of the image, and calculated their radial distribution functions g(r), and the nearest neighbor distance.

2.5. TEM characterization and chemical identification

In order to image the microgel monolayer and identify the chemical species present in it, we performed TEM, High-Angle Annular Dark-Field imaging (STEM-HAADF), and Energy-Dispersive X-ray Spectroscopy (EDS) measurements (Thermo Fisher Scientific TALOS F200X) with an acceleration voltage of 200 kV. To reproduce the deposition procedure described in the previous section, microgels were deposited from the water/air interface at $\Pi \simeq 20\ mN\,m^{-1}$ into a copper TEM grid, and dried at room temperature. While we cannot ensure that Π is exactly the same as for silicon substrates due to the deposition process, this serves as a first approximation to characterize self-assembled monolayers. The details on the sample preparation are presented in Supplementary Materials.

2.6. XPS measurements

The surface chemistry of the deposited monolayers was characterized by means of X-ray Photoelectron Spectroscopy (XPS, PHI VersaProbe II equipped with a monochromated Al X-Ray source for excitation at 1486.6 eV) with an analyzing spot diameter of 200 μm. The data treatment and peak fitting was done using the *XPSPeak* software.

2.7. Plasma etching

Air plasma etching was applied to the deposited microgels to test their resistance to plasma etching in the presence of POM^{3-}. Measurements were done by means of a radio frequency plasma device (KX1050 Plasma Asher, Emitech). Substrates with deposited microgels were subjected to air plasma during 30 minutes at 100 W and characterized by AFM before and after the treatment.

3. Results and discussion

Characterizing the electrophoretic mobility, μ_e, of a microgel dispersion is useful to determine the accumulation of different type of ions on the microgels. This allows to compare how the electric state of the surface of the microgels changes depending on the nature of the ions present in solution [20]. In Fig. 1 we present the μ_e trend from 25 °C to 49 °C for a dispersion of positively charged microgels in the presence of 10^{-4} M of POM^{3-}. In order to make comparisons, we also performed this characterization in the absence of salt, and with 10^{-4} M of NaCl. The green curve without salt at pH 3 showed positive μ_e values as expected for the positive charge of our microgels, with no significant changes after adding 10^{-4} M of NaCl. Around the VPTT, 33.7 ± 0.2 °C, there was an increase in μ_e due to the deswelling of the microgel, which resulted in more charges per unit of area. This scenario significantly changes in the presence of POM^{3-} at 10^{-4} M. In this case, the electrophoretic mobility inverted its sign, which means a charge inversion of the pNIPAM microgels in all range of temperatures studied. The negative electrokinetic charge in the presence of POM^{3-} increased as the microgel deswelled, reaching a value even higher, in absolute value, than the positive μ_e reached with NaCl at 10^{-4} M. We previously observed charge inversion with the monovalent tetraphenil borate anion (Ph_4B^-) at 10^{-3} M, but only above the VPTT, where the microgels show a more hydrophobic nature [19]. The charge reversal in the swollen state of the pNIPAM, when the microgel is more hydrated, shows that the POM^{3-} also strongly accumulates in the pNIPAM interface in its more hydrophilic state. Our results confirm that the POM^{3-} anions show a strong interaction with positive pNIPAM microgels in both the more hydrophilic and more hydrophobic states, below and above the VPTT, respectively. This high ionic specificity is beyond the one of a pure electrostatic interaction, and it has been ascribed to its dual character of ion and nanocolloid [37,38] or to superchaotropicity [39].

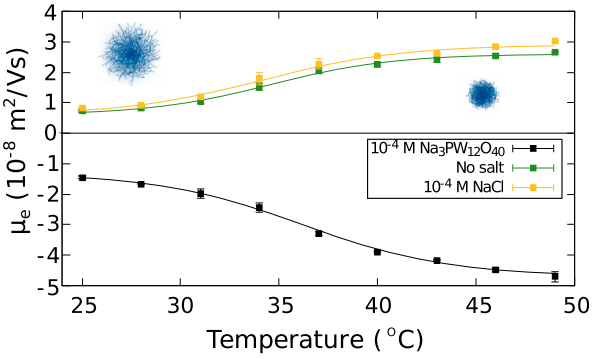

Fig. 1. a) Electrophoretic mobility (μ_e) as a function of temperature for positively charged pNIPAM microgels at pH 3 in the absence of salt (■), with 10^{-4} M of NaCl (■), and 10^{-4} M of POM^{3-}, (■). The lines are guides to the eye.

Next, we conducted μ_e and hydrodynamic diameter D_h measurements as a function of the POM^{3-} concentration for positively and negatively charged microgels. For the positively charged microgels at 25 °C, the results in Fig. 2a showed no significant changes on the microgel charge below 10^{-5} M. At $5 \cdot 10^{-5}$ M we found the isoelectric point indicating a full screening of the microgel charge. By increasing the POM^{3-} concentration, a strong absorption of POM^{3-} was observed as the μ_e became negative. Above $5 \cdot 10^{-5}$ M, despite existing an electrostatic repulsion between the already negative microgel and the POM^{3-} anions, the value of μ_e kept decreasing, which we hypothesize it might be mediated by both the softness of the swelled microgels that would allow for more anions to keep absorbing onto them, and the ionic specific effects between POM^{3-} and the microgels. This hypothesis is supported by reference measurements done with slightly negatively charged microgels. In Fig. 2c it can be seen how the μ_e of negatively charged microgels became more negative upon increasing the POM^{3-} concentration, despite existing an electrostatic repulsion. As we will discuss, the D_h measurements in Fig. 2b and d reinforce this hypothesis.

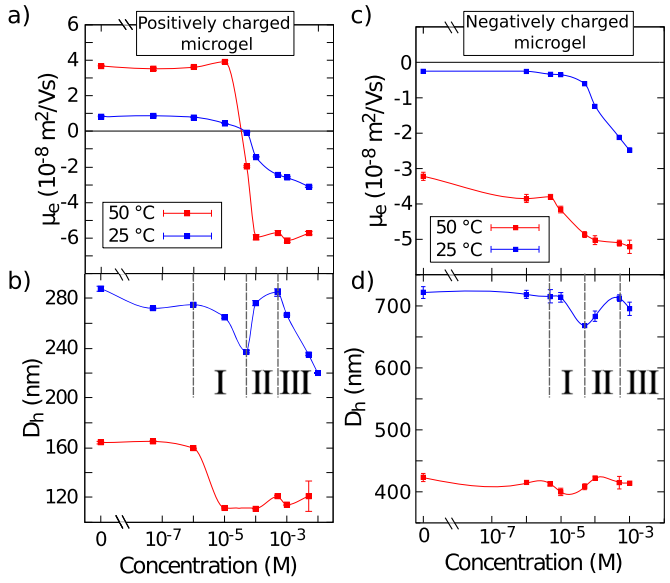

Fig. 2. Electrophoretic mobility μ_e and hydrodynamic diameter D_h for the **a-b)** positively charged microgels and **c-d)** negatively charged microgels as a function of the concentration of POM^{3-} at 25 °C (■), and at 50 °C (■). The lines are guides to the eye.

For the positively charged microgels at 50 °C, the microgels deswelled with the corresponding increase in charge per unit area, exhibiting the same trend in μ_e as at 25 °C. However, at $5 \cdot 10^{-5}$ M we already observed a charge inversion which significantly increased as the POM^{3-} concentration increased up to 10^{-4} M. Beyond that point, further increases in POM^{3-} concentration were not reflected on the μ_e, which remained constant. These results seem to indicate that the interaction of the POM^{3-} with the pNIPAM was even stronger in its deswollen state. These results are in good agreement with our previous studies on the adsorption of POM^{3-} and charge inversion for hard nanoparticles, where we observed a stronger interaction of POM^{3-} when surfaces were more hydrophobic [38]. For the negatively charged microgels in Fig. 2c, the accumulation of POM^{3-} on the microgel above the VPTT was also evidenced as the μ_e decreased regardless of the electrostatic repulsion between the POM^{3-} anion and the negative microgel.

We show the influence of POM^{3-} concentration on the size of positively charged microgels in Fig. 2b. At 25 °C, a deswelling-swelling-deswelling trend was observed. This is a striking behavior found for both positively and negatively charged microgels (see Fig. 2c and d). Thus, this effect happens regardless of the role of POM^{3-}, either acting as counter-ion or co-ion, in Fig. 2b and 2d, respectively. This hints to a strong binding of POM^{3-} anions to pNIPAM polymers regardless of the overall charge of the microgels, although the effect appears stronger when acting as a counter-ion as seen in Fig. 2c. The later is expected as the electrostatic interaction enhances the counter-ion absorption onto the pNIPAM. We propose that this non-monotonic behavior might result from a rather complex competition of two interactions: i) the absorption of POM^{3-} tends to dehydrate the pNIPAM chains, causing their collapse, and ii) the accumulation of POM^{3-} anions tend to re-swell the microgels due to electrostatic repulsion. We have labeled each regime in Fig. 2b and d as I-II-III, in order to gain clarity in the discussion. We will particularize first to the positively charged microgels, since the behavior is similar to the negatively charged one, but stronger in terms of size variation. In Fig. 2b regime I, the size of the positively charged microgels decreased 17.7% from 288 ± 2 nm to 237 ± 1 nm at $5 \cdot 10^{-5}$ M, where a minimum in D_h was observed, at the same POM^{3-} concentration where we observed the isoelectric point in Fig. 2a. We previously found that it is possible to deswell the pNIPAM microgels below the VPTT thanks to ionic specific interactions [40]. Nevertheless, on that study we used simpler ions belonging to the Hofmeister series. Moreover, the concentration of ions at which microgels begun to deswell were always above $3 \cdot 10^{-1}$ M, significantly higher than those used here. In a recent work, Brasili et al. found that the absorption of oppositely charged gold nanoparticles led to a deswelling caused by the screening of the microgel charge [41]. As explained above, the deswelling observed for our microgels might be due to a dehydration of the pNIPAM chains induced by the binding of POM^{3-}. When POM^{3-} is absorbed on the microgel, a competition for the water molecules between the pNIPAM chains and the POM^{3-} occurs, resulting in a partial dehydration of the chains [40,42]. By increasing the POM^{3-} concentration we enter regime II, where the great absorption of POM^{3-} on the microgels resulted in their re-swelling, reaching the original D_h at $5 \cdot 10^{-4}$ M. This happened at the corresponding POM^{3-} concentration where μ_e showed a charge reversal in Fig. 2a. Our working hypothesis for this behavior is that this reswelling comes from both the electrostatic repulsion between the POM^{3-} anions absorbed inside the microgel, and the increase in the charge of the microgel [43]. This re-swelling was not previously observed with the ions belonging to the Hofmeister series. This points out to a stronger and more complex interaction of POM^{3-} anions with the positively charged pNIPAM microgels. Therefore, it is plausible that at such low concentrations as 10^{-4}M, the effect produced by the overcharging is greater than the dehydration observed in regime I, resulting in the observed re-swelling. Finally, in regime III, we found that increasing the POM^{3-} concentration above 10^{-3} M resulted again in a partial deswelling of the microgels. At 10^{-3} M POM^{3-}, the concentration seems to be sufficiently high for the dehydration effect described in regime I to now overcome the electrostatic repulsion provided by the absorbed POM^{3-} anions, which tends to swell the microgel in regime II. The same three regimes corresponding to the non-monotonic deswelling-swelling-deswelling were also observed for the negatively and more crosslinked microgels at similar POM^{3-} concentrations. Once more, this behavior confirms the strong ionic specific interactions between the microgels and the POM^{3-}, where the latter absorbs in the negative microgel in its swollen state regardless of the existing electrostatic repulsion.

We now focus on the behavior above the VPTT in Fig. 2b and d, at 50 °C, particularizing first to the positively charged microgels. The most relevant result was the further deswelling of the microgels at 10^{-5} M indicating that the microgel expelled even more water above the VPTT due to the presence of the POM^{3-} anions. It should be noted that this deswelling appears at a concentration at which μ_e was still positive in Fig. 2a. This further $\simeq 30\%$ size reduction remained constant in all tested POM^{3-} concentrations above 10^{-5} M. Previous studies with pNIPAM microgels showed a sequential deswelling upon heating, where the difference in the electrokinetic temperature and the volume phase transition temperature pointed out to a first deswelling of the shell, followed by a further deswelling of the core [43,44]. Authors evidenced this sequential deswelling from a minimum in the R_g/R_h ratio [43,44]. However, in our case, the further deswelling occurred at 50 °C, well above the VPTT where the microgel was already in a deswollen state. To our knowledge, this is the first time that such significant 30% further deswelling above the VPTT has been observed. In any case, it is worth noting that the further deswelling upon POM^{3-} absorption above the VPTT that we report here is mediated by a different mechanism. When comparing to the negatively charged microgels in Fig. 2d, we did not observe significant variations in the D_h compared to the positively charged microgels, although the μ_e showed that POM^{3-} anions kept accumulating on both microgels thanks to the strong specific interactions. This difference might come from the more rigid nature of the negatively charged microgels above the VPTT, due to their higher crosslinking density, more than 4.5 times compared to the positively charged microgels, and the absence of co-monomers providing additional charges to the polymeric network.

The analysis of the μ_e and D_h data vs POM^{3-} concentration shows enhanced effects for the positively charged microgels, with a charge

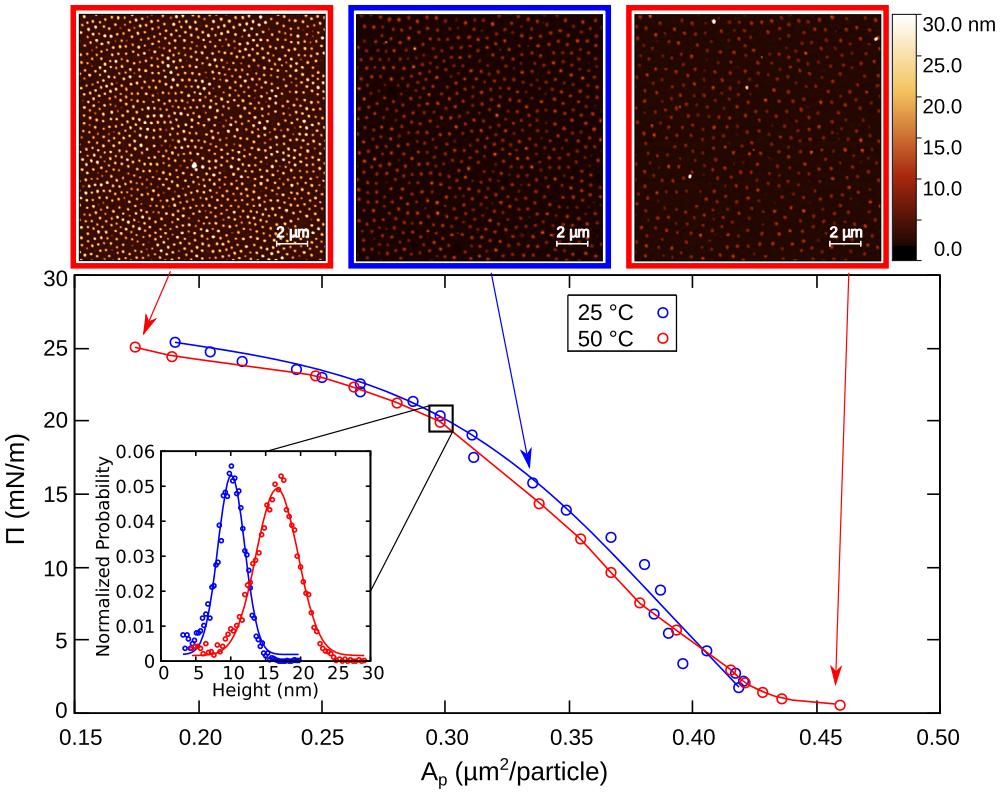

Fig. 3. Surface pressure Π versus area per particle A_p and representative AFM images obtained by the simultaneous compression and deposition of a monolayer of positively charged microgels from a water/air interface on a silicon wafer. The inset shows the microgel height distributions measured with AFM at Π ≃20 mN m^{-1} for 25 °C (•) and 50 °C (•). The color of the images frames showcases the temperature at which microgels were deposited at. The lines are guides to the eye.

inversion and further deswelling above the VPTT. In this case, the POM^{3-} acts as a counter-ion favoring both the electrostatic and specific effect interactions, and the microgel is softer compared to the more crosslinked negative microgel. Therefore, this points to the two main ingredients to control these ionic specific interactions: charge and softness.

In order to compare the effect of the electrostatic charge, we conducted additional experiments with another Keggin type polyoxometalate, $H_4SiW_{12}O_{40}$ (POM^{4-}) and the positively charged microgels in Fig. S3. In addition, it is known that POM^{4-} remains stable at pH < 4.5, and thus it is stable at our working conditions of pH 3 [33]. These measurements can contribute to shed light about the possible influence that the lacunary species, $PW_{11}O_{39}^{7-}$, might have on the observed results with POM^{3-}.

In Fig. S3a, the μ_e results showed almost no differences between the POM^{3-} and the POM^{4-}, both below and above the VPTT, showing that the increase in charge from POM^{3-} to POM^{4-} did not significantly alter the overall electric state of the microgels. The D_h in Fig. S3b also showed the same trend for both POMs, with a greater reswelling for POM^{4-} at 25 °C. This is consistent with our hypothesis, where the reswelling arises from the electrostatic repulsion between the POMs absorbed in the microgel. Since the POM^{4-} has a greater negative charge than POM^{3-}, the repulsion between the POM^{4-} anions inside the microgel increases, resulting in the enhanced reswelling observed at 25 °C. Both the reswelling and the final deswelling occurred for both POMs at the same concentration. This points out to the accumulation not being only caused by an electrostatic attraction [45]. Above the VPTT, at 51 °C, the two-step deswelling was also observed in the presence of POM^{4-}.

As stated above, at pH 3 the POM^{3-} is not totally stable, and some percentage might be present as lacunary species, such as $PW_{11}O_{40}^{7-}$ (POM^{7-}) [33]. The latter has a negative charge of -7, greater than the -4 charge of the POM^{4-}. If the lacunary POM^{7-} was the main specie the electrostatic repulsion would result in a higher reswelling compared to POM^{4-}. Thus, it seems reasonable to state that in our working conditions the lacunary species had no major impact in the observed effects.

Next, we will discuss the effect of the interaction of POM^{3-} anions with positively charged pNIPAM microgels confined at water/air interfaces. To this end, we performed Langmuir-Blodgett experiments, where the monolayers were transferred to silicon substrates and characterized by atomic force microscopy (AFM). In these experiments, both the subphase in the Langmuir trough and the microgel dispersion were kept at pH 3 and at the same POM^{3-} concentration.

Recent studies showed a plethora of new behaviors happening when microgels are confined at 2D fluid interfaces [9]. Therefore, before analyzing the role of POM^{3-}, we characterized the compression curve of our bare positively charged microgels at pH 3 without salt, below and above the VPTT (see Fig. 3, and Fig. S4-S5).

The adsorption of microgels at water/air interfaces is a process out of thermodynamic equilibrium, hence our denomination of a compression curve instead of a compression isotherm. This is because slightly different amounts of deposited microgels at the interface lead to different compression curves, making comparisons difficult or meaningless when only attending to the total mass of the microgels assumed to be deposited at the interface. With our method of measuring the ex-situ area per particle for each value of Π we avoid this problem and we can compare between different experiments and conditions.

We reproduced the behavior for small microgels that we reported in a previous work [46], where rather monodisperse small microgels (PDI ≤ 0.1, measured by DLS) self-assembled into a glass at the interface due to small variations of their internal polymeric network. This provided polydispersity in the soft steric repulsive interactions at the interface that frustrated the crystallization of the monolayer, as seen in Fig. 3. We also reproduced the results of a previous work finding that the microgels did not change their diameter at the interface regardless

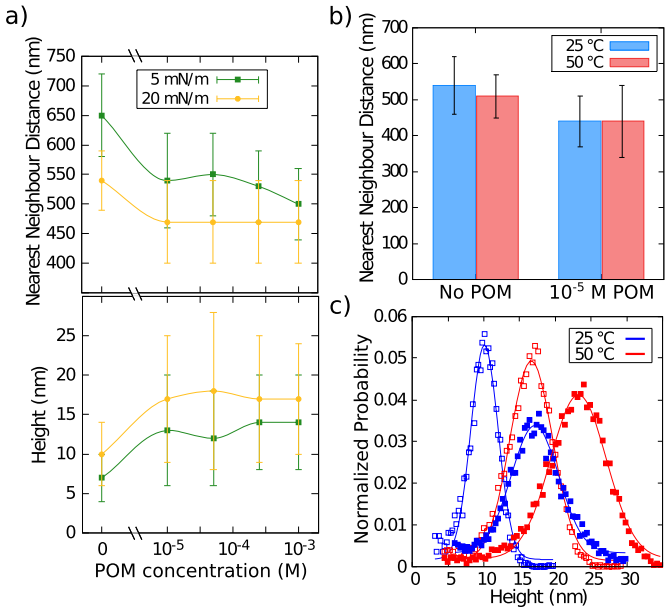

Fig. 4. a) Nearest Neighbor Distance (NND) in positively charged microgel monolayers (top) and maximum height of the microgels (bottom) vs POM^{3-} concentration at $\Pi = 5$ (■) and 20 mN m^{-1} (♦), at 25 °C. **b)** NND at $\Pi = 20$ mN m^{-1} of microgels without POM^{3-} (left) and with 10^{-5} M POM^{3-} (right), at 25 °C (blue) and 50 °C (red). **c)** Maximum height of microgels distribution at $\Pi = 20$ mN m^{-1}, open symbols correspond to measurements in the absence of salt at 25 °C (□) and 50 °C (□), while solid symbols are in the presence of 10^{-5} M of POM^{3-} at 25 °C (■) and 50 °C (■). Lines are guides to the eye.

of being above or below the VPTT [12,14], as reflected by the overlapping compression curves at 25 and 50 °C. The portion immersed in the subphase was still thermoresponsive, resulting in the deswelling of that portion above the VPTT, which was reflected in an increase in height of the microgel after the deposition on the silicon substrate (see the inset in Fig. 3). Therefore, a higher height after the deposition is a signature of deswelling of the portion immersed in the subphase before the deposition.

As explained in the introduction, recent new experimental evidence has reported the role of charges on microgels confined at fluid interfaces, in this case by changing the pH of pH-responsive microgels [3]. Our present study aims to contribute to fill the gap on the role of ionic specificity in the behavior of microgels confined at fluid interfaces. By size, our microgels would be "small microgels" according to our previous study [46] and the one by Schmidt et al. [3].

In Fig. 4a, we studied the role of the ionic specificity of the POM^{3-} in the self-assembly of positively charged microgels confined at liquid interfaces at 5 and 20 mN m^{-1} at 25 °C, i.e. below the VPTT. We tracked the position of each microgel in the AFM images (see Supplementary Materials for details), and we characterized the nearest neighbor distance (NND), which reflects the diameter of the microgels at the water/air interface. In addition, we determined the maximum height of the deposited microgel monolayers as the average of this value for all the microgels in an image. The uncertainty associated to each measurement was calculated from the Full Width at Half Maximum (FWHM) of the height and NND distributions. This uncertainty appeared as a consequence of the polydispersity of the microgels at the interface [12].

In the absence of POM^{3-}, in Fig. 4a we found the expected compression of the monolayer from 5 to 20 mN m^{-1}, with the NND being reduced by 17% from 650±70 nm to 540±40 nm, and the maximum height increasing by 43% from 7±3 nm to 10±4 nm. When the POM^{3-} was added at 10^{-5} M, the microgels at 5 mN m^{-1} reduced their NND by 17%, down to 540±80 nm, and increased their height by 85% up to 13 ± 7 nm. Hence, the NND and height of the deposited microgels at 5 mN m^{-1} in the presence of 10^{-5} *M* POM^{3-} exhibited similar values as the microgels deposited at 20 mN m^{-1} in the absence of POM^{3-}. In other words, the addition of POM^{3-} at such low concentration as 10^{-5} M produced an effect on the microgel monolayer which was equivalent to mechanically compressing it from 5 to 20 mN m^{-1}. As the concentration of POM^{3-} increased above 10^{-5} M, the NND and height remained almost constant, reflecting that at 10^{-5} M the effect produced by the POM^{3-} on the microgels at the interface already saturated. This behavior was different to the one observed for the microgels in bulk in Fig. 2a and b, where in the range of the concentrations measured significant variations of the μ_e and D_h were observed. Interestingly, Schmidt et al. found a decrease in the diameter of small microgels at the interface upon pH-swelling [3]. Our results go in a different direction since the decrease in diameter in the presence of POM^{3-} was accompanied by a deswelling of the portion immersed in the subphase, reflected in an increase of height after the deposition.

We also measured the effect of NaCl in the self assembly of the microgels at the interface in order to compare with the POM^{3-} results. Measurements with NaCl were carried out at 10^{-1} M, 100 times more concentrated than the most concentrated tested POM^{3-} solution. If we would like to compare ionic strengths then the NaCl concentration has to be divided by 6. We did not find any changes in either the NND nor the heights of the microgels with respect to the absence of salt (Fig. S6, and Table S4). This evidences that the results obtained with POM^{3-} came from the strong ionic specific interactions with pNIPAM microgels. This strong affinity was also reflected in an onset of effects at similar concentrations both in bulk and at the interface.

In Fig. 4b-c, we investigated the effect of temperature for microgel monolayers in the presence of POM^{3-}. In the absence of POM^{3-}, we observed similar values of NND below and above the VPTT, as discussed in Fig. 3 [3,14]. Similarly, by adding 10^{-5} M of POM^{3-}, the NND remained equal below and above the VPTT, but with a lower value than in the case of no POM^{3-}, as already shown in Fig. 4a. Furthermore, we observed a two-step height increase in Fig. 4c, in accordance to the two-step deswelling shown in bulk in Fig. 2b. First, the deswelling of the swollen core of the microgel when the temperature was above the VPTT in the absence of salt only affected the height of the deposited microgels, increasing it when compared to their corresponding depositions at 25 °C. Next, the addition of POM^{3-} at 25 °C increased the height of the deposited microgels, matching the one achieved by heating the sample above the VPTT in the absence of POM^{3-}, as reflected by the overlapping distribution functions in Fig. 4c. Thus, by adding 10^{-5} M of POM^{3-} we accomplished an effect equivalent to heating above the VPTT. Furthermore, when we heated the sample in the presence of POM^{3-} up to 50 °C, we observed a further increase in their height up to 23 ± 9 nm. As explained above, these results are in good agreement with the two-step deswelling observed in bulk in Fig. 2b, where the further deswelling observed for the microgels in bulk above the VPTT was reflected in a further increase of the height of the deposited microgels in Fig. 4c.

As discussed above, POM^{3-} anions are not interfacially active, but their confinement at the interface was promoted by the interfacial activity of the microgels [23,47]. Therefore, it is reasonable to expect an accumulation of the POM^{3-} anions both at the liquid interface where the coronas of the microgels are stretched, and in the respective portions still immersed in the subphase. Nevertheless, the confinement of the microgels at the liquid interface restricts their ability to re-arrange, which could cause the saturation of the effects observed. It is reasonable to expect that with more crosslinked, i.e. stiffer, microgels the effects produced by the POM^{3-} might be weaker. The opposite might occur for less crosslinked, i.e. softer, microgels. This might be compared with the constant size observed in bulk above the VPTT, where the microgel is more rigid and therefore has less ability to re-arrange. There, the POM^{3-} kept adsorbing on the microgel when the concentration was increased, as reflected in the decrease of μ_e between 10^{-5} M and 10^{-4} M in Fig. 2a. However, this increased absorption of the POM^{3-} was not reflected on the size in Fig. 2b, where the deswelling effect produced by the POM^{3-} already saturated at 10^{-5} M.

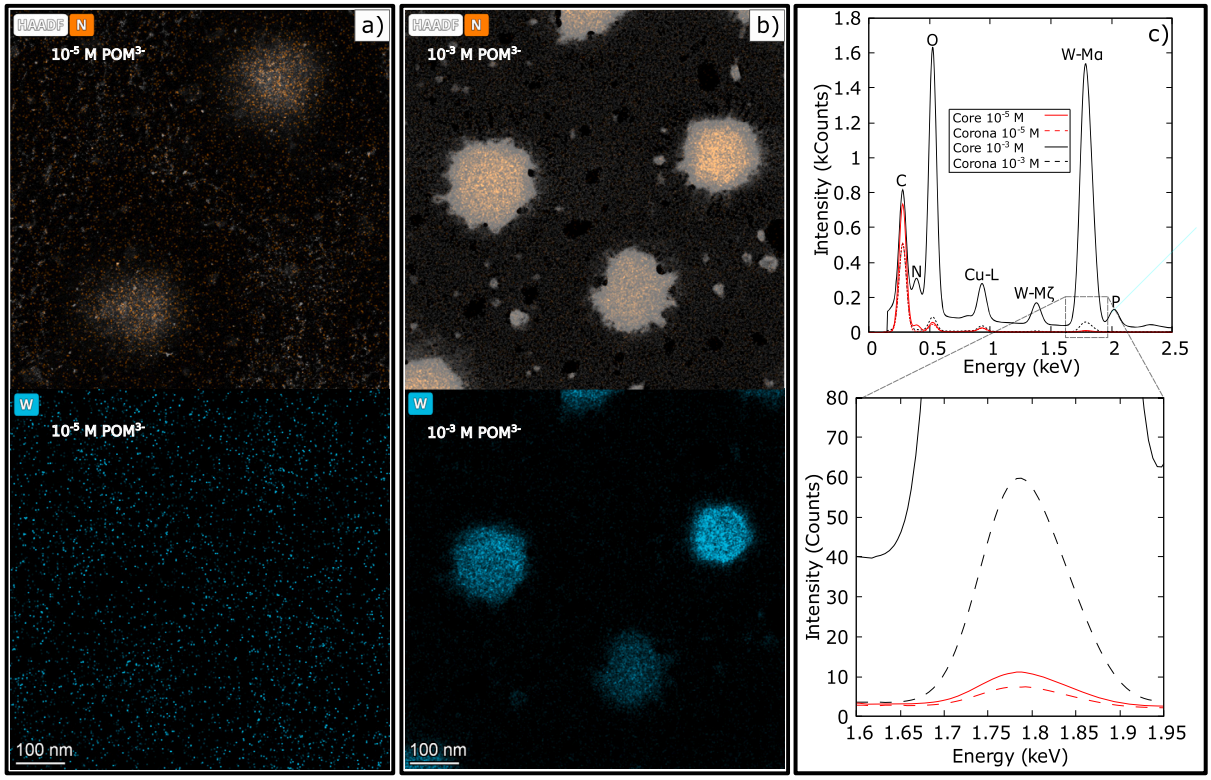

Fig. 5. HAADF-STEM images and EDS mapping of the positively charged microgel monolayers deposited at $\Pi \simeq 20$ mN m^{-1} with **a)** 10^{-5} M of POM^{3-} and **b)** 10^{-3} M of POM^{3-}. Top row pictures show N mapping, while bottom row pictures show W mapping. **c)** Spectra obtained from EDS. Solid/dashed lines correspond to the core and corona of a deposited microgel in a-b, respectively. Red/black color corresponds to 10^{-5} M and 10^{-3} M POM^{3-} concentrations, respectively. The bottom image shows a zoom-in of the region of interest for 10^{-5} M.

In order to locate the distribution and amount of POM^{3-} in the pNIPAM microgels, we characterized the location of the pNIPAM and POM^{3-} anions on the deposited monolayers by HAADF-STEM and EDS (see details in Materials, Supplementary Materials and Fig. S7, S8, and S9). Since the POM^{3-}, $[PW_{12}O_{40}]^{3-}$, contains tungsten (W), we used it as an indicator of the POM^{3-} concentration, while nitrogen (N) was used as an indicator of the presence of pNIPAM. It is important to note that the STEM sample preparation resulted in the imaging of a single monolayer of microgels. In Fig. 5a-b, we present the HAADF-STEM and EDS mapping of the microgels deposited at $\Pi \simeq 20$ mN m^{-1} in the presence of 10^{-5} and 10^{-3} M of POM^{3-}, respectively. In both Figures the denser and more cross-linked core revealed a higher N concentration than in the surrounding stretched corona. While it is difficult to see by eye in Fig. 5a, Fig. 5b shows that the POM^{3-} was accumulated both at the microgel core and the stretched corona, with more POM^{3-} on the core compared to the stretched corona. To illustrate this greater absorption on the core of the microgel, Fig. 5c shows the corresponding EDS spectra in the core of one of the microgels compared to its corona (see more details in Fig. S10, S11, S12 and S13). In the zoom-in, it is possible to see how the signal corresponding to the $W - M\alpha$ peak of the EDS spectra was greater in the core region of the microgel also for 10^{-5} M of POM^{3-}.

These results confirm that at 10^{-3} M there was more POM^{3-} accumulation compared to 10^{-5} M. Nevertheless, the effects produced on the deswelling of the portion of the microgel immersed in the subphase, and on the decrease of the diameter at the interface, already saturated at 10^{-5} M, as shown in Fig. 4a through the NND and height of the deposited monolayers characterized by AFM. Hence, the sensitivity of these techniques enabled us to distinguish the accumulation of POM^{3-} in the microgel monolayers as its concentration increased.

Moreover, we also observed some results that point out a restructuring of the microgel polymer network by the presence of POM^{3-}, an effect observed for free pNIPAM chains in bulk [25]. For example, in Fig. S9b, the bridging of two microgel cores is accompanied by the presence of a higher concentration of POM^{3-} in the pNIPAM bridge. This bridging was never observed in the absence of POM^{3-} (see Fig. 3, S4 and S5). Therefore, compared to free pNIPAM chains in bulk [25], the restructuring ability of the POM^{3-} would be significantly reduced when interacting with microgels due to the cross-linked polymer network, but it seems to be still present (see Fig. S14).

We further studied the integrity of the POM^{3-} anions after the deposition of a microgel monolayer from the water/air interface onto the silicon substrates by XPS (see details in the Supplementary Materials). The presence of $W^{(6+)}4f_{7/2}$ and $W^{(6+)}4f_{5/2}$ doublet peaks at binding energies of 35.95 and 38.00 eV revealed the presence of unaltered WO_3, indicating that the POM^{3-} structure remained unaltered [48].

Table 1
XPS analysis with atomic percentages of the elements present in a substrate with positively charged microgels deposited at $\Pi = 20$ mN m^{-1} at 25 °C with 10^{-5} M POM^{3-}. The relative concentrations of each peak from the deconvoluted spectra of $W4f$ are also shown, where $W^{(5+)}$ corresponds to partially degraded POM^{3-}.

Signal (Binding Energy, eV)	(%)
$C1s$ (285.03)	28.25
$N1s$ (399.92	3.7
$O1s$ (532.21)	33.1
$Si2p$ (98.99)	33.9
$W4f$	0.7
XPS fitting of the W4f Spectra	**(% relative to the W4f signal)**
$W^{(6+)}4f_{7/2}$ (35.95)	41.0
$W^{(6+)}4f_{5/2}$ (38.00)	30.8
$W^{(6+)}4p_{3/2}$ (40.91)	5.9
$W^{(5+)}4f_{7/2}$ (34.45)	12.7
$W^{(5+)}4f_{5/2}$ (36.44)	9.6

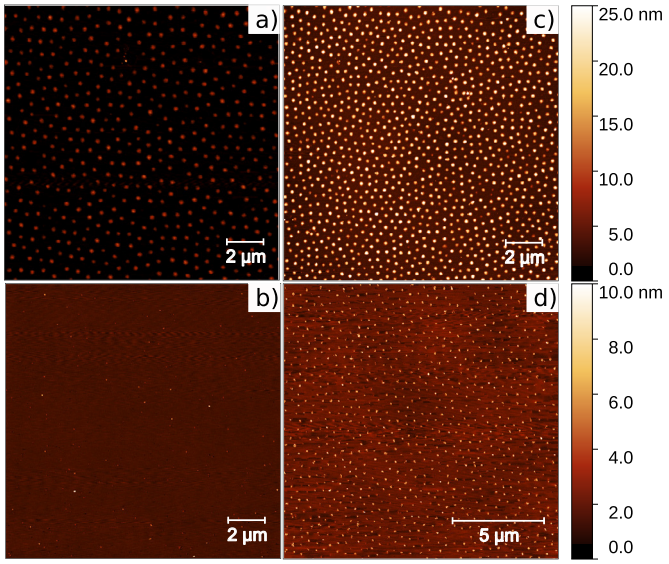

Fig. 6. Showcase of the improved ability of microgels to perform as lithography masks by resisting more to an air plasma treatment of 30 min at 100 W. AFM images obtained by the deposition of positively charged microgels at 20 mN m^{-1}. Depositions were done in the absence (a-b) and presence (c-d) of POM^{3-} at 10^{-5} M. AFM images were acquired before (a-c) and after (b-d) the plasma treatment.

A slight reduction into the W^{5+} oxidation state was observed as new $W^{(5+)}4f_{7/2}$ and $W^{(5+)}4f_{5/2}$ signals appeared at 34.45 and 26.44 eV, respectively, signaling the partial degradation of the POM^{3-} (see Fig. S15). We present the relative concentration of each element for the analyzed sample in Table 1 at 10^{-5} M of POM^{3-}, showing that $\simeq 22\%$ of the POM^{3-} partially degraded during the harsh process of depositing and drying on a silicon substrate.

Finally, to showcase if the microgels restructured by POM^{3-} improved their ability to perform as lithography masks, we subjected microgel monolayers to plasma etching to compare their resistance to be etched. As discussed in the introduction, the height of the produced vertically aligned nanowires will be determined by the resistance of microgels to etching [11]. Thus, more resistance of the lithography masks to plasma etching would result in higher vertically aligned nanowires during a dry etching process.

To do this, substrates with positively charged microgels deposited at $\Pi = 20$ mN m^{-1} with no POM^{3-} and with 10^{-5} M POM^{3-} were subjected to air plasma at 100 W for 30 min. We acquired AFM images before and after the treatment. In Fig. 6, it is visible the compression of the monolayer induced by the POM^{3-}, with a reduction of the NND and brighter, i.e. higher, microgels. Height distribution profiles of the micrographs in Fig. 6 are shown in Fig. S16. After the plasma treatment, we noticed that the addition of 10^{-5} M POM^{3-} prevented the full etching of the monolayer. We believe that the addition of POM^{3-} results in more rigid and denser microgels that can resist the plasma etching for longer times. This would hint to an improved performance as lithography masks by plasma dry etching.

4. Conclusion

In this paper we show evidences of the strong interaction between positively and negatively charged pNIPAM microgels and Keggin-type $[PW_{12}O_{40}]^{3-}$ and $[SiW_{12}O_{40}]^{4-}$ anions (POM^{3-} and POM^{4-}) in bulk, and we examine the behavior at the water/air interface of the positively charged microgels in the presence of POM^{3-}.

Ionic specificity effects were observed at low concentrations of POM^{3-} (ca. $5 \cdot 10^{-5}$ M) for both microgels, below and above the VPTT. In bulk, we observed charge inversion of the positively charged microgels in all temperatures investigated, specially in the deswollen state. Below the VPTT, the hydrodynamic diameter D_h exhibited a non-monotonic deswelling-swelling-deswelling trend with the POM^{3-} concentration for both microgels. We propose a mechanism to explain such complex behavior that involves two interactions: i) the dehydration of the pNIPAM chains due to the absorption of the POM^{3-} anions, and ii) the electrostatic repulsion between POM^{3-} anions that appears when the concentration is high enough. Above the VPTT, we observed a novel *extra* 30% deswelling of the positively charged microgel at 10^{-5} M of POM^{3-}. While the later was not present for the negatively charged microgels, the electrophoretic mobility μ_e showed that the POM^{3-} kept absorbing also on these microgels even when the POM^{3-} acts as a co-ion. These novel results are a consequence of the great interaction of POM^{3-} with the pNIPAM microgels, as it has been reported for free pNIPAM chains in bulk [25]. We also conclude the important role of the softness of the microgels below and above the VPTT, with effects that cannot be explained considering the microgels above the VPTT as hard particles [1].

At the water/air interface, the interaction of 10^{-5} M POM^{3-} with the positively charged microgel monolayers below the VPTT resulted in a decrease of the diameter of the microgels at the interface and a deswelling of the portion immersed in the subphase. The later was reflected in a height increase of the deposited microgels. In the absence of POM^{3-}, it was necessary to compress from 5 to 20 mN m^{-1} to achieve an equal reduction in the diameter, and to heat above the VPTT to observe similar values in the increased height. Above the VPTT, we only observed an extra deswelling of the portion immersed in the subphase when POM^{3-} was added, in agreement with the results in bulk. The monolayer behavior did not change above 10^{-5} M of POM^{3-}, indicating a saturation effect, despite the further accumulation of POM^{3-} on the pNIPAM characterized by EDS mapping. We propose an explanation for this saturation effect and the one observed in bulk for the D_h above the VPTT. In both cases, the microgel ability to re-arrange, i.e. its softness, is restricted either due to the confinement at the water/air interface or due to the deswelling above the VPTT in bulk. This restriction in the softness would be responsible for the observed saturation effects.

As a general conclusion, this work points out the importance of the ionic specific interactions over the tuning of the bulk behavior and 2D interfacial self-assembly of pNIPAM microgels below and above the VPTT. It stands out that the behavior of soft matter in presence of ionic specificity effects is richer and more complex than those with hard colloidal particles [49]. Hence, to obtain a deeper understanding at molecular level on the interaction between POM^{3-} and pNIPAM microgels, further experiments including molecular dynamics simulations are required. In addition, we have already envisioned a possible application of this type of interaction in the improvement of soft colloidal lithography, since the microgel monolayers showed improved resistance to plasma etching.

CRediT authorship contribution statement

Antonio Rubio-Andrés: Writing – review & editing, Writing – original draft, Visualization, Validation, Investigation, Data curation. **Delfi Bastos-González:** Writing – review & editing, Writing – original draft, Supervision, Resources, Methodology, Conceptualization. **Miguel Angel Fernandez-Rodriguez:** Writing – review & editing, Writing – original draft, Supervision, Software, Resources, Project administration, Methodology, Funding acquisition, Conceptualization.

Declaration of competing interest

The authors declare the following financial interests/personal relationships which may be considered as potential competing interests: Miguel Angel Fernandez-Rodriguez reports financial support was provided by Spain Ministry of Science and Innovation. Miguel Angel

Fernandez-Rodriguez reports financial support was provided by Junta de Andalucía.

Data availability

Data will be made available on request.

Acknowledgements

Funding for open access charge: Universidad de Granada / CBUA. We acknowledge Dr. María Tirado Miranda for providing measurements and helpful insight regarding the DLS technique, and Dr. Jordi Faraudo Gener and Dr. Carlos Drummond for insightful conversations, the CIC from University of Granada for the STEM-HAADF and EDS measurements, and the SCAI from the University of Málaga for the XPS measurements. This work was supported by the projects PID2020-116615RA-I00 funded by MCIN/AEI/ 10.13039/501100011033, and EMERGIA grant with reference EMC21_00008, and projects PY20-00241, A-FQM-90-UGR20 funded by Consejería de Universidad, Investigación e Innovación de la Junta de Andalucía, and by FEDER "ERDF A way of making Europe".

Appendix A. Supplementary material

Supplementary material related to this article can be found online at https://doi.org/10.1016/j.molliq.2024.124496.

References

[1] L.A. Lyon, A. Fernandez-Nieves, The polymer/colloid duality of microgel suspensions, Annu. Rev. Phys. Chem. 63 (2012) 25–43.
[2] K. Naseem, R. Begum, W. Wu, M. Usman, A. Irfan, A.G. Al-Sehemi, Z.H. Farooqi, Adsorptive removal of heavy metal ions using polystyrene-poly (N-isopropylmethacrylamide-acrylic acid) core/shell gel particles: adsorption isotherms and kinetic study, J. Mol. Liq. 277 (2019) 522–531.
[3] M.M. Schmidt, S. Bochenek, A.A. Gavrilov, I.I. Potemkin, W. Richtering, Influence of charges on the behavior of polyelectrolyte microgels confined to oil–water interfaces, Langmuir 36 (37) (2020) 11079–11093.
[4] H.M. Crowther, B.R. Saunders, S.J. Mears, T. Cosgrove, B. Vincent, S.M. King, G.-E. Yu, Poly (nipam) microgel particle de-swelling: a light scattering and small-angle neutron scattering study, Colloids Surf. A, Physicochem. Eng. Asp. 152 (3) (1999) 327–333.
[5] I. Varga, T. Gilányi, R. Mészáros, G. Filipcsei, M. Zrínyi, Effect of cross-link density on the internal structure of poly (n-isopropylacrylamide) microgels, J. Phys. Chem. 105 (38) (2001) 9071–9076.
[6] B.R. Saunders, On the structure of poly (n-isopropylacrylamide) microgel particles, Langmuir 20 (10) (2004) 3925–3932.
[7] M. Destribats, V. Lapeyre, M. Wolfs, E. Sellier, F. Leal-Calderon, V. Ravaine, V. Schmitt, Soft microgels as pickering emulsion stabilisers: role of particle deformability, Soft Matter 7 (17) (2011) 7689–7698.
[8] F. Camerin, M.A. Fernandez-Rodriguez, L. Rovigatti, M.-N. Antonopoulou, N. Gnan, A. Ninarello, L. Isa, E. Zaccarelli, Microgels adsorbed at liquid–liquid interfaces: a joint numerical and experimental study, ACS Nano 13 (4) (2019) 4548–4559.
[9] M.A. Fernandez-Rodriguez, A. Martín-Molina, J. Maldonado-Valderrama, Microgels at interfaces, from mickering emulsions to flat interfaces and back, Adv. Colloid Interface Sci. 288 (2021) 102350.
[10] M.-C. Tatry, P. Galanopoulo, L. Waldmann, V. Lapeyre, P. Garrigue, V. Schmitt, V. Ravaine, Pickering emulsions stabilized by thermoresponsive oligo (ethylene glycol)-based microgels: effect of temperature-sensitivity on emulsion stability, J. Colloid Interface Sci. 589 (2021) 96–109.
[11] M.A. Fernandez-Rodriguez, M.-N. Antonopoulou, L. Isa, Near-zero surface pressure assembly of rectangular lattices of microgels at fluid interfaces for colloidal lithography, Soft Matter 17 (2) (2021) 335–340.
[12] S. Bochenek, A. Scotti, W. Ogieglo, M.Á. Fernández-Rodríguez, M.F. Schulte, R.A. Gumerov, N.V. Bushuev, I.I. Potemkin, M. Wessling, L. Isa, et al., Effect of the 3d swelling of microgels on their 2d phase behavior at the liquid–liquid interface, Langmuir 35 (51) (2019) 16780–16792.
[13] S. Bochenek, F. Camerin, E. Zaccarelli, A. Maestro, M.M. Schmidt, W. Richtering, A. Scotti, In-situ study of the impact of temperature and architecture on the interfacial structure of microgels, Nat. Commun. 13 (1) (2022) 1–12.
[14] J. Harrer, M. Rey, S. Ciarella, H. Löwen, L.M. Janssen, N. Vogel, Stimuli-responsive behavior of PNiPAm microgels under interfacial confinement, Langmuir 35 (32) (2019) 10512–10521.
[15] J. Vialetto, Novel insights on the three-dimensional shape of microgels at fluid interfaces, Chimia 76 (10) (2022) 852.
[16] Y. Zhang, S. Furyk, D.E. Bergbreiter, P.S. Cremer, Specific ion effects on the water solubility of macromolecules: PNIPAM and the Hofmeister series, J. Am. Chem. Soc. 127 (41) (2005) 14505–14510.
[17] T. López-León, J.L. Ortega-Vinuesa, D. Bastos-González, A. Elaissari, Thermally sensitive reversible microgels formed by poly (N-isopropylacrylamide) charged chains: a Hofmeister effect study, J. Colloid Interface Sci. 426 (2014) 300–307.
[18] E. Daly, B.R. Saunders, A study of the effect of electrolyte on the swelling and stability of poly (n-isopropylacrylamide) microgel dispersions, Langmuir 16 (13) (2000) 5546–5552.
[19] L. Pérez-Fuentes, C. Drummond, J. Faraudo, D. Bastos-González, Anions make the difference: insights from the interaction of big cations and anions with poly (N-isopropylacrylamide) chains and microgels, Soft Matter 11 (25) (2015) 5077–5086.
[20] D. Bastos-González, L. Pérez-Fuentes, C. Drummond, J. Faraudo, Ions at interfaces: the central role of hydration and hydrophobicity, Curr. Opin. Colloid Interface Sci. 23 (2016) 19–28.
[21] D.C. Malaspina, C. Viñas, F. Teixidor, J. Faraudo, Atomistic simulations of cosan: amphiphiles without a head-and-tail design display "head and tail" surfactant behavior, Angew. Chem., Int. Ed. 59 (8) (2020) 3088–3092.
[22] J.-H. Kruse, M. Langer, I. Romanenko, I. Trentin, D. Hernández-Castillo, L. González, F.H. Schacher, C. Streb, Polyoxometalate-soft matter composite materials: design strategies, applications, and future directions, Adv. Funct. Mater. (2022) 2208428.
[23] M. Hohenschutz, I. Grillo, O. Diat, P. Bauduin, How nano-ions act like ionic surfactants, Angew. Chem. 132 (21) (2020) 8161–8165.
[24] L. Girard, B. Naskar, J.-F. Dufrêche, J. Lai, O. Diat, P. Bauduin, A thermodynamic model of non-ionic surfactants' micellization in the presence of polyoxometalates, J. Mol. Liq. 293 (2019) 111280.
[25] T. Buchecker, P. Schmid, I. Grillo, S. Prévost, M. Drechsler, O. Diat, A. Pfitzner, P. Bauduin, Self-assembly of short chain poly-N-isopropylacrylamid induced by superchaotropic Keggin polyoxometalates: from globules to sheets, J. Am. Chem. Soc. 141 (17) (2019) 6890–6899.
[26] J. Simons, M. Hohenschutz, W. Richtering, Tailoring non-ionic microgel swelling by nano-ion binding, in: 18th Zsigmondy Colloquium, 2023, p. 29.
[27] A. Gil, J.J. Carbó, Computational modelling of the interactions between polyoxometalates and biological systems, Front. Chem. 10 (2022).
[28] R. Liu, C. Streb, Polyoxometalate-single atom catalysts (POM-SACs) in energy research and catalysis, Adv. Energy Mater. 11 (25) (2021) 2101120.
[29] A. Bijelic, M. Aureliano, A. Rompel, Polyoxometalates as potential next-generation metallodrugs in the combat against cancer, Angew. Chem., Int. Ed. 58 (10) (2019) 2980–2999.
[30] H. Soria-Carrera, I. Franco-Castillo, P. Romero, S. Martín, J.M. de la Fuente, S.G. Mitchell, R. Martín-Rapún, On-POM ring-opening polymerisation of N-carboxyanhydrides, Angew. Chem. 133 (7) (2021) 3491–3495.
[31] J. Xu, Z. Zhu, T. Su, W. Liao, C. Deng, D. Hao, Y. Zhao, W. Ren, H. Lʹu, Green aerobic oxidative desulfurization of diesel by constructing an Fe-Anderson type polyoxometalate and benzene sulfonic acid-based deep eutectic solvent biomimetic cycle, Chin. J. Catal. 41 (5) (2020) 868–876.
[32] M. Ammam, Polyoxometalates: formation, structures, principal properties, main deposition methods and application in sensing, J. Mater. Chem. A 1 (21) (2013) 6291–6312.
[33] N.I. Gumerova, A. Rompel, Polyoxometalates in solution: speciation under spotlight, Chem. Soc. Rev. 49 (21) (2020) 7568–7601.
[34] L.H. Alvarez, A.A. Rudov, R.A. Gumerov, P. Lenssen, U. Simon, I.I. Potemkin, D. Wöll, Controlling microgel deformation via deposition method and surface functionalization of solid supports, Phys. Chem. Chem. Phys. 23 (8) (2021) 4927–4934.
[35] J.G. Guerrero-Felix, J. Lopez-Miras, M.A. Rodriguez-Valverde, C.L. Moraila-Martinez, M.A. Fernandez-Rodriguez, Automation of an atomic force microscope via arduino, HardwareX 15 (2023) e00447.
[36] J.C. Crocker, D.G. Grier, Methods of digital video microscopy for colloidal studies, J. Colloid Interface Sci. 179 (1) (1996) 298–310.
[37] A. Malinenko, A. Jonchère, L. Girard, S. Parrès-Maynadié, O. Diat, P. Bauduin, Are keggin's POMs charged nanocolloids or multicharged anions?, Langmuir 34 (5) (2018) 2026–2038.
[38] C. Drummond, L. Pérez-Fuentes, D. Bastos-González, Can polyoxometalates be considered as superchaotropic ions?, J. Phys. Chem. C 123 (47) (2019) 28744–28752.
[39] K.I. Assaf, W.M. Nau, The chaotropic effect as an assembly motif in chemistry, Angew. Chem., Int. Ed. 57 (43) (2018) 13968–13981.
[40] T. López-León, A. Elaïssari, J.L. Ortega-Vinuesa, D. Bastos-González, Hofmeister effects on poly (nipam) microgel particles: macroscopic evidence of ion adsorption and changes in water structure, ChemPhysChem 8 (1) (2007) 148–156.
[41] F. Brasili, G. Del Monte, A. Capocefalo, E. Chauveau, E. Buratti, S. Casciardi, D. Truzzolillo, S. Sennato, E. Zaccarelli, Toward a unified description of the electrostatic assembly of microgels and nanoparticles, ACS Appl. Mater. Interfaces (2023).
[42] T. López-León, J.L. Ortega-Vinuesa, D. Bastos-González, A. Elaïssari, Cationic and anionic poly (N-isopropylacrylamide) based submicron gel particles: electrokinetic properties and colloidal stability, J. Phys. Chem. 110 (10) (2006) 4629–4636.
[43] R. Elancheliyan, G. Del Monte, E. Chauveau, S. Sennato, E. Zaccarelli, D. Truzzolillo, Role of charge content in the two-step deswelling of poly (n-isopropylacrylamide)-based microgels, Macromolecules 55 (17) (2022) 7526–7539.
[44] G. Del Monte, D. Truzzolillo, F. Camerin, A. Ninarello, E. Chauveau, L. Tavagnacco, N. Gnan, L. Rovigatti, S. Sennato, E. Zaccarelli, Two-step deswelling in the vol-

ume phase transition of thermoresponsive microgels, Proc. Natl. Acad. Sci. 118 (37) (2021) e2109560118.
[45] K. Besteman, M.A. Zevenbergen, H.A. Heering, S.G. Lemay, Direct observation of charge inversion by multivalent ions as a universal electrostatic phenomenon, Phys. Rev. Lett. 93 (17) (2004) 170802.
[46] L. Scheidegger, M.Á. Fernández-Rodríguez, K. Geisel, M. Zanini, R. Elnathan, W. Richtering, L. Isa, Compression and deposition of microgel monolayers from fluid interfaces: particle size effects on interface microstructure and nanolithography, Phys. Chem. Chem. Phys. 19 (13) (2017) 8671–8680.
[47] P. Tang, J. Hao, Formation mechanism and morphology modulation of honeycomb hybrid films made of polyoxometalates/surfactants at the air/water interface, J. Colloid Interface Sci. 333 (1) (2009) 1–5.
[48] X. Cheng, P. Sun, S. Zhang, D. Sun, B. Jiang, W. Wang, X. Xin, Self-assembly of m-phenylenediamine and polyoxometalate into hollow-sphere and core-in-hollow-shell nanostructures for selective adsorption of dyes, J. Mol. Liq. 287 (2019) 110982.
[49] J. Faraudo, A. Moncho-Jordá, D. Bastos-González, C. Drummond, Interaction-limited aggregation: fine-tuning the size of pnipam particles by association with hydrophobic ions, Macromolecules 56 (6) (2023) 2246–2257.